2008

Thermal Model for a Li-Ion Cell

Karthikeyan Kumaresan

Godfrey Sikha
University of South Carolina - Columbia

Ralph E. White
University of South Carolina - Columbia, white@cec.sc.edu

Publication Info

Published in *Journal of the Electrochemical Society*, Volume 155, Issue 2, 2008, pages A164-A171.

Journal of The Electrochemical Society, **155** (2) A164-A171 (2008)
0013-4651/2007/155(2)/A164/8/$23.00 © The Electrochemical Society

Thermal Model for a Li-Ion Cell

Karthikeyan Kumaresan,* Godfrey Sikha, and Ralph E. White***,z**

Department of Chemical Engineering, University of South Carolina, Columbia, South Carolina 29208, USA

A thermal model for a lithium-ion cell is presented and used to predict discharge performance at different operating temperatures. The results from the simulations are compared to experimental data obtained from lithium-ion pouch cells. The model includes a set of parameters (and their concentration and temperature dependencies) that has been obtained for a lithium-ion cell composed of a mesocarbon microbead anode, $LiCoO_2$ cathode in 1 M $LiPF_6$ salt, in a mixture of ethylene carbonate, propylene carbonate, ethyl-methyl carbonate, and diethyl carbonate electrolyte. The parameter set was obtained by comparing the model predictions to the experimental discharge profiles obtained at various temperatures and rates. The concentration and temperature dependence of the extracted parameters were correlated through empirical expressions. Also, the effect of including the thermal dependence of various parameters in the model on the simulated discharge profiles is discussed.
 [DOI: 10.1149/1.2817888]

Manuscript submitted March 28, 2007; revised manuscript received October 23, 2007.
Available electronically December 18, 2007.

The comparison of experimental charge and discharge data with mathematical models helps battery engineers to understand how various parameters—thermodynamic, kinetic, and design—determine the performance of the battery under various operating conditions such as charge/discharge rate, temperature, etc., and to use the model along with the parameters determined from the above comparison to explore the performance of the battery under different operating conditions, thus reducing the experimental efforts required. Such comparisons have been made for batteries of various chemistries[1-5] and the estimated parameters have been used in optimizing those batteries for different intended end uses. In all of the above efforts, the comparisons have been done for experimental data obtained at room-temperature conditions using isothermal models. Due to the lack of experimentally measured data, empirical correlations describing the temperature and concentration dependence of transport properties such as salt-diffusion coefficient, transference number, and mean molar activity of salt have not been used in most of the existing thermal models.[6,7] Moreover, the mean molar salt activity was assigned a constant value of one under the assumption that there is no significant interaction between the constituents of the liquid electrolyte. Recent experimental characterization[8] of transport properties of $LiPF_6$ in a solvent mixture of propylene carbonate/ethylene carbonate/dimethyl carbonate (PC/EC/DMC) reveals that the transport properties, diffusion coefficient and conductivity, and the nonideality of the electrolyte solution vary with temperature and concentration. The work presented in this paper identifies a set of parameters (and their temperature and concentration dependencies) for a lithium-ion cell model which can be used to simulate its performance at different rates and (starting) temperatures. This is done by incorporating currently available experimentally measured parameters[8] and by estimating the rest of the parameters by comparing the discharge profiles predicted by the model with experimentally measured discharge profiles. Using the parameters obtained, the model is used to demonstrate the effect of the inclusion of thermal dependence of various parameters on the simulated discharge profiles.

Mathematical Model

The mass and charge balance equations given by Doyle et al.[9] and the thermal balance equations developed by Gu et al.[10] are used to describe the temporal and spatial distribution of concentration, potential, and temperature in the cell. In addition, the temperature dependency of various transport and kinetic parameters for which experimental data are available in the literature are also included. In this model, the temperature is coupled with other dependent variables through the heat-generation term and the temperature dependence of various transport and kinetic parameters. A summary of the governing equations and boundary conditions used in this work is given in Appendix A.

Experimental

The experimental discharge data used in this work were obtained using lithium-ion pouch cells supplied by the National Reconnaissance Office. Each cell consisted of four (two-sided) positive electrodes (cathodes) and five (three two-sided and two one-sided) negative electrodes (anodes). The active materials of the positive and negative electrodes are lithium cobalt oxide ($LiCoO_2$) and mesocarbon microbead (MCMB) 2528, respectively, and 1 M $LiPF_6$ in a quaternary solvent mixture of EC, PC, ethyl methyl carbonate (EMC), and dimethyl carbonate (DEC) was used as the electrolyte. Each of the four two-sided positive electrodes was bagged using a Celgard separator. Each of the three two-sided negative electrodes was sandwiched between two positive electrode-containing separator bags, while the two single-sided negative electrodes covered the outer positive electrodes. The entire assembly of anodes, cathodes, and separators was enclosed by a proprietary material to make the pouch cell. The rated capacity of the cell is 1.656 Ah (used as C rate in this paper). After the formation cycles, the charge and discharge capacities of these cells were measured at four different temperatures, 15, 25, 35, and 45°C, and at three different rates, C/33, C/2, and C. Before starting these measurements the cells were discharged at C/33 rate until the voltage reached 3.3 V. For C/33 rate measurement, the cells were charged until the voltage reached 4.1 V and discharged to 3.3 V, with 30 min rest between these two steps. For C/2 and C rates, the cells were charged at respective current until the voltage reached 4.1 V and were held at the same voltage until the current tapered down to 50 mA. The subsequent discharge was done at the respective constant current until the cell voltage reached 3.3 V and left in open circuit for 30 min. It was followed by a C/33 discharge until the voltage reached 3.3 V to make sure that the subsequent charge started at the same state of charge. All of the above charge/discharge measurements were done using Arbin BT-2000 battery testing systems. Tenny Environmental Chambers (model T6S) were used for maintaining respective temperatures and near-zero humidity atmospheres.

To obtain the open-circuit potential vs state-of-charge profiles of $LiCoO_2$ and MCMB, half-cell tests were conducted. Three electrode half cells were assembled with either $LiCoO_2$ or MCMB as working electrode and lithium as reference and counter electrode. The ring-shaped reference lithium was placed concentrically around the circumference of the working electrode. In this arrangement, the working and counter electrodes were separated by two layers of separators, whereas the working and reference electrodes were separated by a single layer of separator. Before measuring the open-

* Electrochemical Society Student Member.
** Electrochemical Society Active Member.
*** Electrochemical Society Fellow.
z E-mail: white@engr.sc.edu

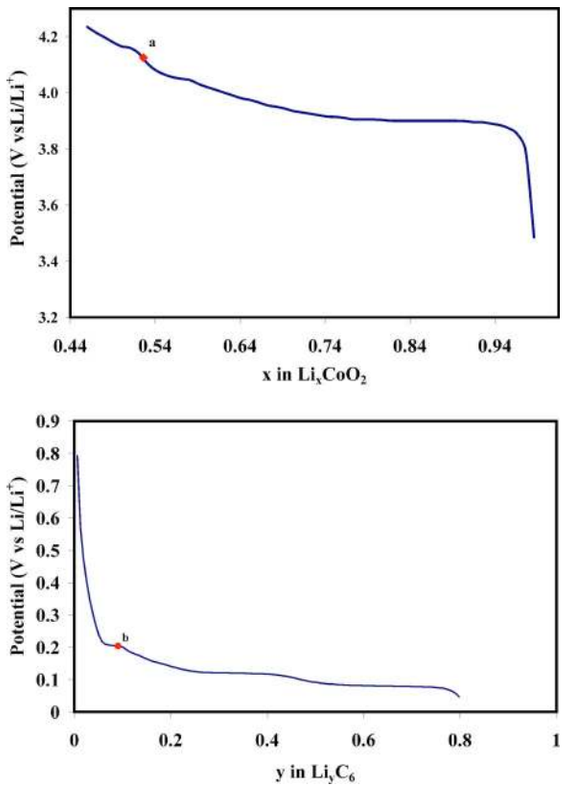

Figure 1. (Color online) Open-circuit potential vs state-of-charge profile of (a) $LiCoO_2$ and (b) MCMB.

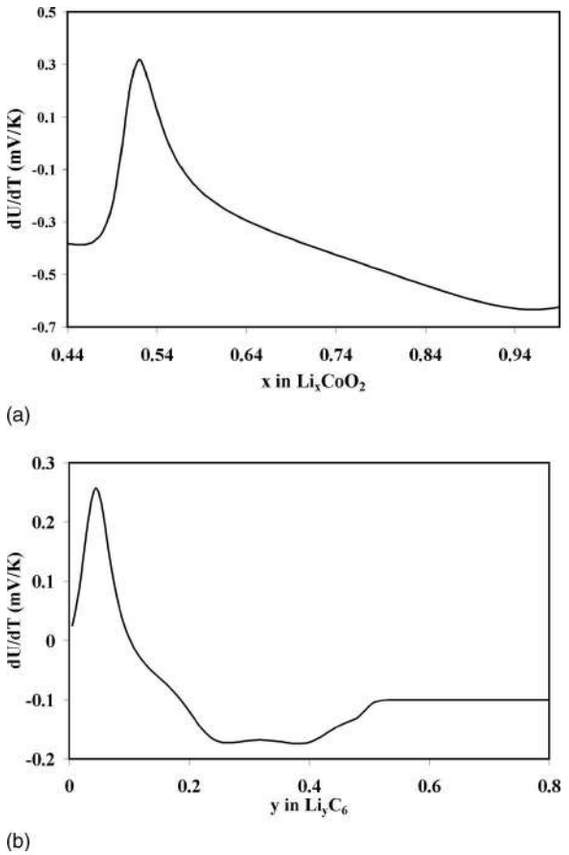

Figure 2. Entropy of (a) Li_xCoO_2 and (b) MCMB as a function of state of charge.[9]

circuit potential the cells were subjected to eight cycles at C/10 rate to make sure that the solid-electrolyte interface (SEI) formation was completed. The open-circuit potential measurements were done at C/60 rate for $LiCoO_2$ and C/70 rate for the MCMB. All the formation cycles and the open-circuit potential measurements were done at room temperature (25°C). Figures 1a and b show the open-circuit potential vs state-of-charge profiles of $LiCoO_2$ and MCMB, respectively. The open-circuit potential of $LiCoO_2$ was measured during the intercalation process, whereas for MCMB it was measured during the deintercalation process.

Under low to moderate rates of discharge, a significant part of total heat generated is due to reversible entropy of reaction (resulting from intercalation and deintercalation of Li^+ ions).[11,7] So, experimentally measured entropy-of-reaction values as a function of state of charge for $LiCoO_2$ (Fig. 2a) and MCMB (Fig. 2b) reported by Thomas and Newman[11] were included in this model. Reynier et al.[12] have shown that the open-circuit potential of graphite electrode, at a given state of charge, has a linear dependence on the temperature between 0 and 23°C. Thomas and Newman[11] also have reported that the open-circuit potentials of both MCMB and $LiCoO_2$ vary linearly with temperature between 21 and 29°C. Moreover, the measurement of entropy of intercalation reaction for both MCMB and $LiCoO_2$ by the above authors[11] have been done based on the assumption that the respective open-circuit potentials are linear functions of temperature. Using the above assumption and the data from Fig. 1 and 2, the open-circuit potentials of the individual electrodes (U_i) at a given temperature are written as follows

$$U_i = U_{i,ref} + (T - T_{ref})\frac{\partial U_i}{\partial T} \quad i = n,p \qquad [1]$$

Here $U_{i,ref}$ is the open-circuit potential of electrode i at the reference temperature, T_{ref}, which is 25°C.

The temperature and concentration dependencies of the properties of the electrolyte system used in this work ($LiPF_6$ in EC/PC/EMC/DEC) have not been reported in the literature. However, Valoen et al.[8] have reported the experimentally measured transport properties (conductivity, salt-diffusion coefficient, transference number, and mean molar activity coefficients) as functions of temperature and salt concentrations for $LiPF_6$ in EC/DMC/PC. The correlations given by these authors were used as initial approximations for estimating the parameters of the system under consideration. A good fit between the model and experiments was obtained by using the same correlations given by the authors for conductivity and salt-diffusion coefficient, while different correlations were used for the dependence of cationic transference number and mean molar activity coefficients. The concentration and temperature dependencies of the ionic conductivity and salt-diffusion coefficients are shown in Fig. 3a and b. The design parameters of the battery are given in Table I.

Parameter Estimation

Initial state of charge of individual electrodes.— The initial state of charge of the individual electrodes is an important parameter, the accuracy of which determines the accuracy of estimates of all other parameters. The individual electrodes were in a completely discharged state ($y = 0$ in Li_yC_6 and $x = 1$ in Li_xCoO_2) when assembled. During formation cycles, a certain amount of cyclable lithium is lost for the formation of the SEI layer. So, it is difficult to determine the state of charge of individual electrodes when a full cell is charged to a certain end of charge voltage or discharged to a certain end of discharge voltage at the end of formation cycles, as explained in our previous work.[13] The method of using the characteristic points on the open-circuit potential vs state-of-charge pro-

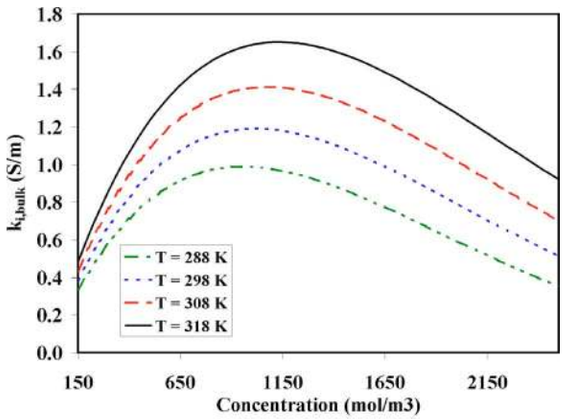

(a)

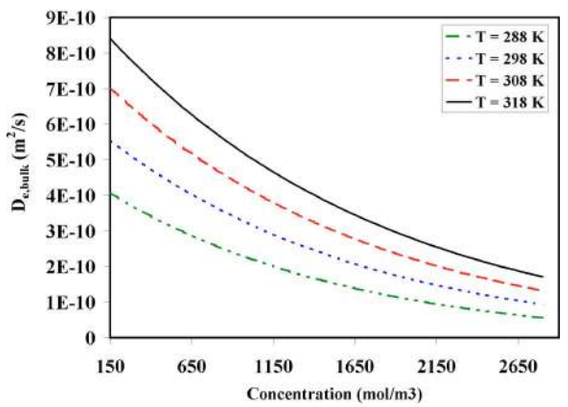

(b)

Figure 3. (Color online) (a) Ionic conductivity and (b) salt-diffusion coefficient as a function of concentration and temperature.[8]

files of individual electrodes as reference points on the slow rate-discharge profiles of full cells is used here to estimate the initial state of charge of individual electrodes. Figure 4 shows the slow (C/33) rate-discharge profile of a full cell at 25°C. Points A and B are the characteristic points of Li_xCoO_2 and Li_yC_6, whose state of charge values can be known from point a in Fig. 1a and b in Fig. 1b, respectively. Using this procedure, the values for the initial state of charge of the individual electrodes were obtained from C/33 rate discharge data and are used as initial conditions in the model for the other rates. In a similar procedure, the initial values for the state of charge of the individual electrodes were estimated for the cells discharged at other temperatures. Figures 5a and b show the discharge

Table I. Design parameters of the cells.

Parameters	Anode (Li_yC_6)	Separator	Cathode (Li_xCoO_2)
Thickness (μm)	73.5	25	70
Particle radius (μm)	12.5	—	8.5
Initial electrolyte concentration (mol/m^3)	—	1000	—
$C_{s,t}$ (mol/m^3)	31,858	—	49,943
Active material density, ρ (kg/m^3)	5031.67	—	2292
ε	0.4382	0.45	0.30
ε_f	0.0566	—	0.15

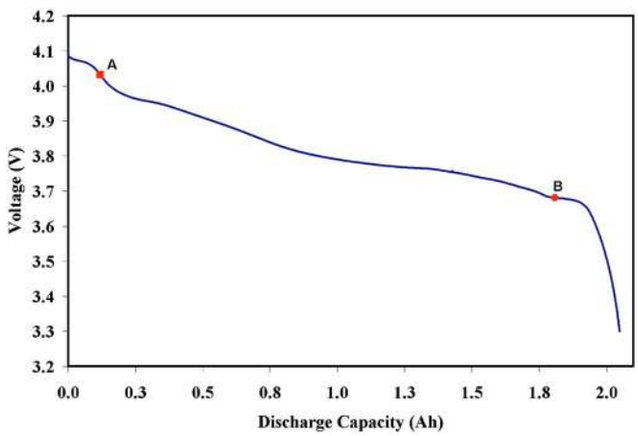

Figure 4. (Color online) C/33 rate-discharge profile of full cell at 25°C. Points A and B here correspond to point a in Fig. 1a and point b in Fig. 1b.

profiles at three different rates at 15 and 45°C, respectively, along with the state of charge of individual electrodes at the beginning and end of discharge.

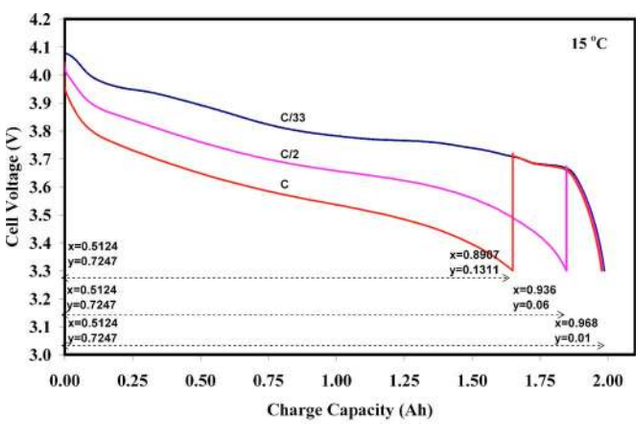

(a)

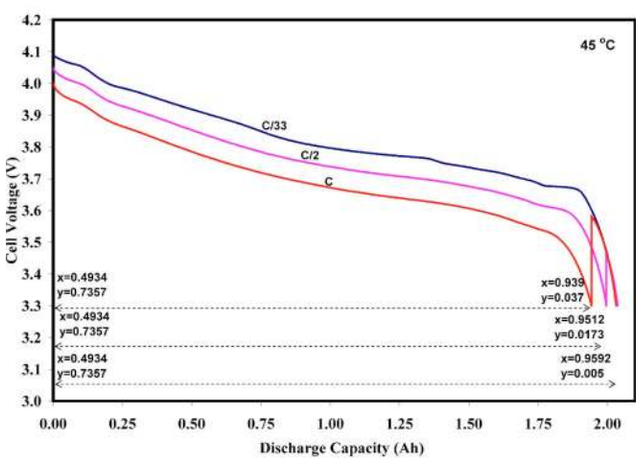

(b)

Figure 5. (Color online) State of charge of individual electrodes at the beginning and at the end of discharge at three different rates (a) at 15 and (b) at 45°C.

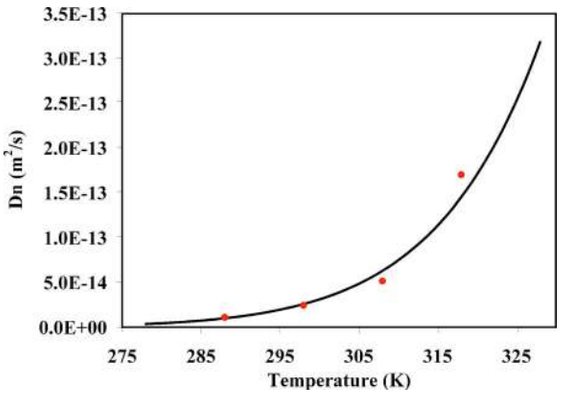

Figure 6. (Color online) Diffusion coefficient of Li in MCMB as a function of temperature. Red dots are the values obtained by comparison between model and experiments and the black solid line is plotted using Eq. 2.

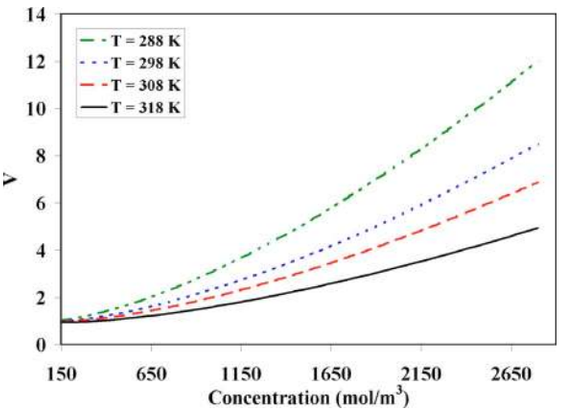

Figure 7. (Color online) Variation of thermodynamic factor V with temperature and salt concentration plotted using Eq. 3a and 3b.

Solid-phase diffusion coefficients.— It has been reported that the value of solid-phase diffusion coefficient of Li in $LiCoO_2$ ($D_{s,p}$) is larger than that in MCMB ($D_{s,n}$) by an order of 3.[3] Based on this observation, and also because $LiCoO_2$ particles (8.5 μm) are smaller than that of MCMB (12.5 μm) in the cell under consideration, it can be assumed that the solid-phase diffusion limitations in the $LiCoO_2$ particle are negligible compared to that in the MCMB particle. It can also be assumed by that having an inherently high value, any change in the value of $D_{s,p}$ with temperature does not change the effect of solid-phase diffusion limitation in the positive electrode. Because the initial state of charge of individual electrodes has already been estimated and the diffusion coefficient of Li in $LiCoO_2$ has been kept constant (1×10^{-11} m^2/s), the diffusion coefficient of Li in MCMB at a given temperature can be estimated by comparing the respective experimental slow (C/33) rate discharge profile to the simulation results. Also, the temperature can be expected to be constant throughout the discharge at this slow rate. Using the four values of $D_{s,n}$ obtained at four different temperatures, an Arrhenius correlation can be derived as given below (Eq. 2) and shown in Fig. 6. The correlation thus obtained can be used in the model for higher rate-discharge simulations, where temperature variations with discharge time could be significant

$$D_{s,n} = 1.4523 \times 10^{-13} \exp\left[\frac{68025.7}{R}\left(\frac{1}{318} - \frac{1}{T}\right)\right] \qquad [2]$$

Nonideality of electrolyte.— The current density in the electrolyte phase of the lithium-ion cell is related to the electrolyte phase potential and electrolyte concentration by the following modified Ohm's law

$$i_2 = -\kappa_i \nabla \phi_2 + \frac{2\kappa_i RT}{F} V \frac{1}{C} \nabla C \qquad [3a]$$

where

$$V = (1 - t^+)\left(1 + \frac{d \ln f_\pm}{d \ln C}\right) \qquad [3b]$$

In previously published models for lithium-ion systems,[1-4] the relationship between the liquid-phase potential drop and the concentration gradient is expressed by Eq. 3a, with $V = (1-t^+)$, instead of Eq. 3b. This implies that the mean molar activity coefficient $f_\pm$ is independent of the concentration of the electrolyte. But, as shown by Valoen et al.,[8] through experimental measurements for the $LiPF_6$ in the PC/EC/DMC system, the mean molar activity coefficient of the salt is a strong function of concentration and temperature. The temperature and concentration dependence of the salt activity coefficient ($f_\pm$) arises due to the short-range ion-solvent interaction. The interaction between the ions and the solvent can be ignored only in a dilute concentration. So, the concentration dependence of ($f_\pm$) can be neglected at low concentration and $V = (1 - t^+)$ can be used instead of Eq. 3b. But, as the concentration of salt increases, the ion-solvent interaction increases, thus increasing the concentration dependency of mean molar activity of the salt. The empirical relationship between the thermodynamic factor V, concentration, and temperature given by these authors was taken as an initial guess for our system and adjusted until a good fit was obtained at C/2 and C/1 rates at all four temperatures (15, 25, 35, and 45°C). The correlation thus obtained is given by Eq. 4 below, and plots obtained using the correlation at four different temperatures are shown in Fig. 7. The values of the thermodynamic factor show the importance of including the nonideality of the electrolyte in the model. In the case where the nonideality of the electrolyte is neglected, the term $V = 1 - t^+$ has a value of 0.6, for a typical value of $t^+ = 0.4$ at room temperature (25°C). But from Fig. 7 it is clear that the value of V can reach as high as 6.0 if the concentration at any point inside reaches 2000 mol/m^3 at room temperature.

$$V = 1.0442 - 0.0132C^{1/2} + 0.5645C^{3/2} + 0.09067T^{1/2}C^{3/2} - 0.0055TC^{3/2} - 0.0001T^{3/2}C^{3/2} \qquad [4]$$

Other parameters.— Other parameters such as surface-reaction kinetic constants (anodic and cathodic transfer coefficients and rate constants) for both anode and cathode, average heat conductivity of anode, separator, and cathode, solid-phase conductivities, Brugge-

Table II. Parameters obtained by comparing the model with experimental discharge profiles.

Parameters	Anode (Li_yC_6)	Separator	Cathode (Li_xCoO_2)
Solid-phase diffusion coefficient (m^2/s)	See Eq. 1[a]	—	1×10^{-11}[b]
α_c	0.5[c]	—	0.5[c]
α_a	0.5[c]	—	0.5[c]
k_i, at 25°C	1.764×10^{-11}[a]	—	6.6667×10^{-11}[a]
Average heat conductivity, λ (W/m/K)	1.7[c]	0.16[c]	2.1[c]
σ (S/m)	100[b]	—	10[b]
brug	4.1[a]	2.3[a]	1.5[a]
t^+		0.435[a]	

[a] Obtained by fit to experimental data.
[b] From Ref. 3.
[c] Assumed value.

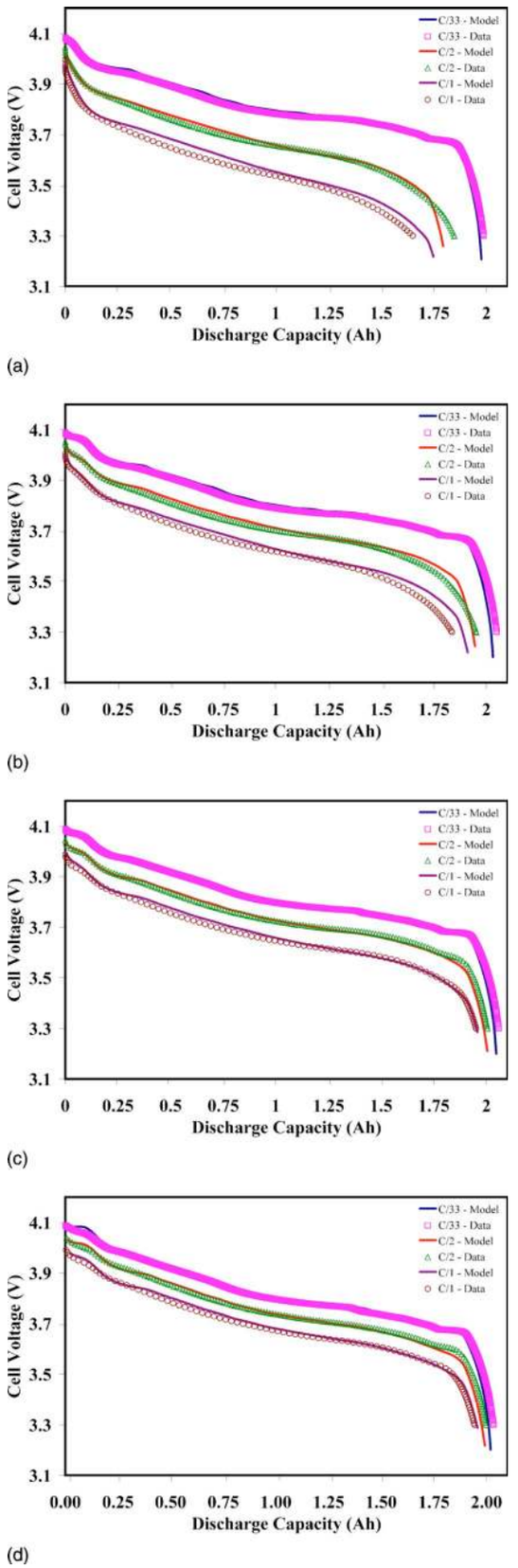

Figure 8. (Color online) Comparison between simulated and experimental discharge profiles at C/33, C/2, and C/1 rates. The experimental data was obtained from lithium-ion pouch cells discharged at corresponding rates to a cut-off potential of 3.0 V: (a) 15, (b) 25, (c) 35, and (d) 45°C.

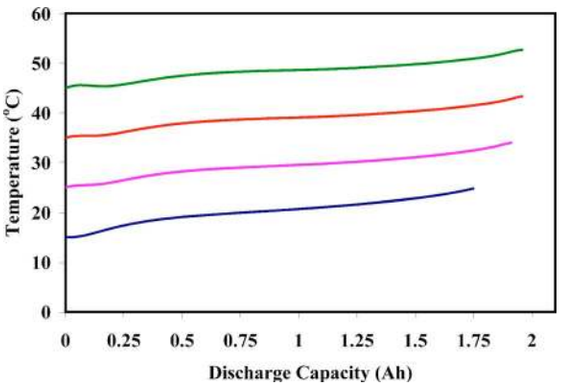

Figure 9. (Color online) Variation of skin temperature of cell with C-rate discharge for different starting temperatures.

man coefficients, and cationic transfer number are given in Table II. The kinetic constants ($k_{i,at\ 25°C}$) shown in Table II were obtained by comparing the model and experimental discharge curves at 25°C. The same values were used to simulate discharge curve at other temperatures also, indicating that the temperature dependence of the rate constants are negligible compared to the temperature dependence of transport properties.

Results and Discussion

The parameters that were obtained as explained in the previous sections can be used to simulate the discharge performance of the lithium-ion cell at various rates and temperatures. Figures 8a-d show the comparison between the simulated and experimental discharge curves at various rates at starting temperatures of 15, 25, 35, and 45°C, respectively. The simulation results show good agreement with the experimental data obtained at different rates and temperatures. The increase in the cell temperature during the discharge process at a given rate depends on the temperature at the beginning of the discharge. The simulated skin temperature of the cell during discharge for different starting temperatures at C rate is shown in Fig. 9. The temperature increase during the entire discharge with a starting temperature of 15°C is 9.8°C, whereas that for a starting temperature of 45°C is only 7.7°C. Figure 9 also reveals that the higher temperature rise in the cells with lower operating temperature occurs in shorter times, thereby indicating a higher rate of heat generation in these cases. This is caused by the steeper concentration and potential gradients that are created across the cell (due to lower transport properties) during discharge at lower temperatures. Because the increase in temperature is significant during higher rates of discharge, the importance of including the temperature dependence of various transport (liquid-phase diffusion coefficient, liquid-phase conductivity, and solid-phase diffusion coefficient in MCMB) and thermodynamic (thermodynamic factor V) parameters in the thermal model are analyzed for C-rate discharge simulations. Figure 10a shows the effect of neglecting the temperature dependence of the thermodynamic factor V on the C-rate discharge profiles with four different initial temperatures (15, 25, 35, and 45°C). For each case, the expression for the thermodynamic factor V was calculated based on the respective initial temperatures. The simulated voltage profiles obtained using these temperature-independent expressions for the thermodynamic factor was compared to the simulated voltage profiles obtained with the temperature-dependent expressions and is shown in Fig. 10a. In all four cases, the model slightly underpredicts the cell voltage near the later part of discharge profile when the thermal dependence of the thermodynamic factor (decrease in thermodynamic factor V with temperature) is dropped. The effect of temperature dependence of liquid-phase conductivity on the simulated discharge profile was found to be negligible, as shown in Fig. 10b. Here, the discharge profiles shown by the broken lines are those

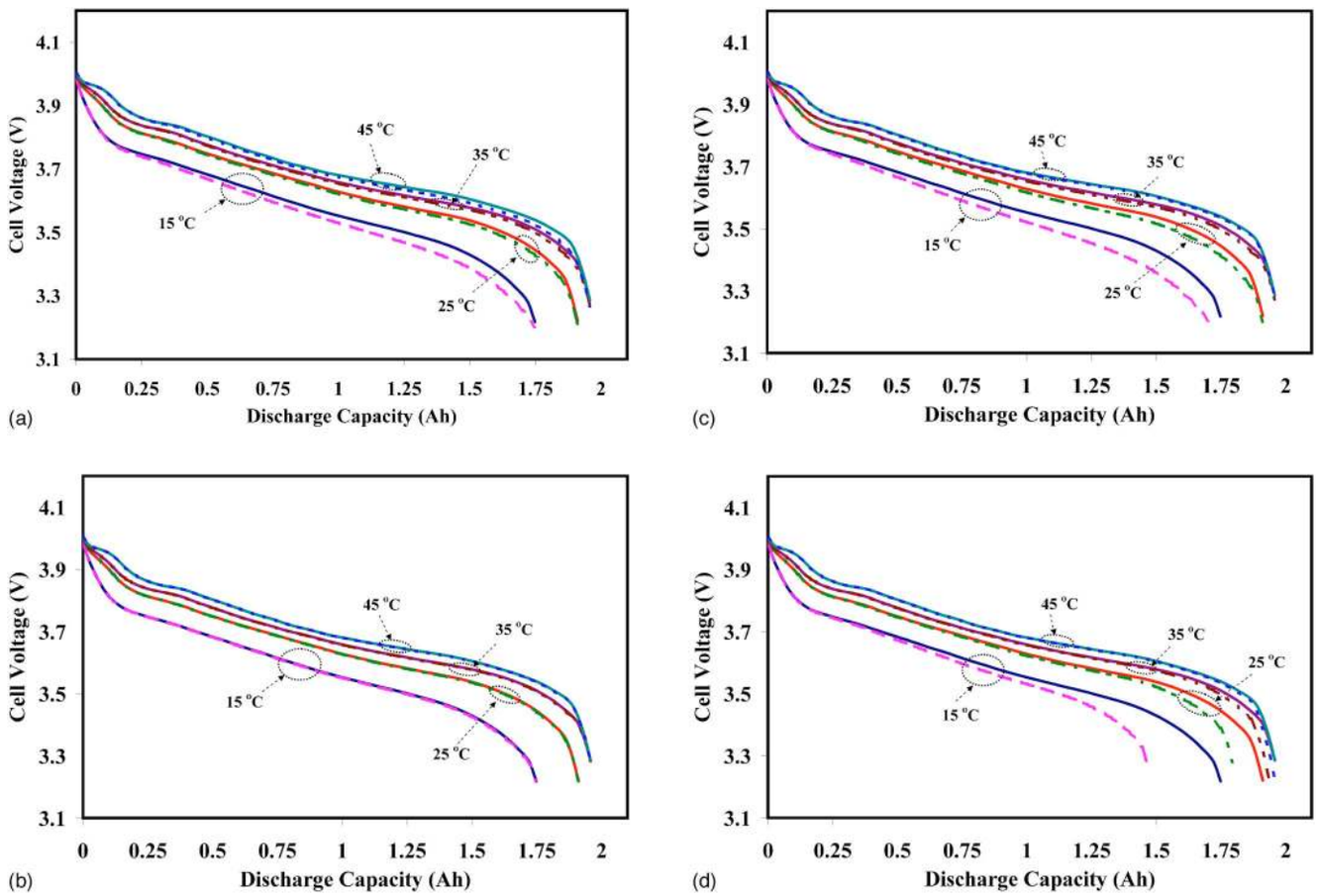

Figure 10. (Color online) Comparison of simulated discharge profiles with and without temperature dependence of different parameters: (a) thermodynamic factor (V), (b) ionic conductivity of electrolyte, (c) salt-diffusion coefficient of the electrolyte, and (d) Solid-phase lithium-diffusion coefficient in MCMB. See text for details.

obtained using the conductivity expression given by Eq. B-2 substituted with respective starting temperatures. Figure 10c compares the C-rate discharge profiles with and without (substituting respective starting temperatures in Eq. B-1) temperature dependence of liquid-phase salt-diffusion coefficient. It is observed that the effect of thermal dependence decreases with increasing starting temperature. This is because, for discharge process with higher starting temperatures, the value of liquid-phase salt-diffusion coefficient at the beginning of the discharge is so high that the increase in value due to temperature rise during discharge does not have a significant effect on diffusion processes. A similar behavior was displayed by the thermal dependence of the solid-phase diffusion coefficient of the negative electrode as shown in Fig. 10d. The purpose of the comparisons made in Fig. 10a-d is to show the effect of thermal dependence of a given parameter due to the temperature increase occurring only during the discharge process. That is, in simulating each of the discharge profiles represented by broken lines, the temperature-independent parameter expressions calculated at the respective starting temperatures were used in the model. In order to understand the importance of using the thermal model with temperature-dependent parameters, the discharge profiles predicted using a complete model are compared (Fig. 11) with the predictions from a model without the temperature dependence of all the transport properties. The solid lines in Fig. 11 are C-rate discharge profiles predicted by the complete model, whereas the broken lines are those obtained using a model with transport properties calculated at respective initial temperatures. Figure 11 shows that a model excluding the temperature dependence of the transport properties may significantly underpredict the discharge capacity of a cell, especially for discharges with low starting temperatures.

Conclusion

A set of parameters has been obtained for a thermal-electrochemical model of a lithium-ion cell by comparing the simu-

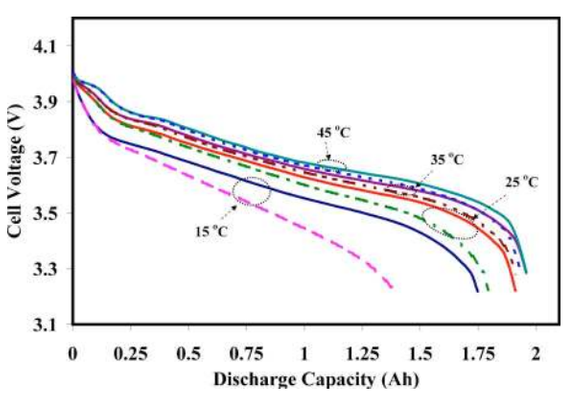

Figure 11. (Color online) Comparison of simulated discharge profiles with and without temperature dependence of all the transport properties.

lated discharge profiles with the experimental discharge data. Along with the parameters obtained here, the model can be used to simulate the discharge performance for a range of starting temperatures (15–45°C) and rates (up to C rate). Using the model and the parameters obtained in this paper, the effect of thermal dependence of four parameters, namely, liquid-phase ionic conductivity, liquid-phase salt-diffusion coefficient, solid-phase diffusion coefficient of negative electrode, and the thermodynamic factor on the simulated C-rate discharge profiles, is analyzed.

Acknowledgments

Financial support for this project provided by the National Reconnaissance Office (contract no. NRO-000-013-C-0122) is gratefully acknowledged.

University of South Carolina assisted in meeting the publication costs of this article.

Appendix A

Governing equations

The model equations describing the nonisothermal discharge and charge process of a lithium-ion battery are as follows: Liquid-phase material balance[7,14]

$$\varepsilon_i \frac{\partial C}{\partial t} = \nabla \cdot (\varepsilon_i D_i \nabla C) + a_i j_{n,i}(1 - t^+), \quad i = n,s,p \qquad [A\text{-}1]$$

Liquid-phase potential

$$i_2 = -\kappa_i \nabla \phi_2 + \frac{2\kappa_i RT}{F} V \frac{1}{C} \nabla C, \quad i = n,s,p \qquad [A\text{-}2a]$$

where $$V = (1 - t^+)\left(1 + \frac{d \ln f_\pm}{d \ln C}\right) \qquad [A\text{-}2b]$$

Solid-phase potential

$$i_1 = -\sigma_i \nabla \phi_1, \quad i = n,p \qquad [A\text{-}3]$$

Conservation of charge

$$\nabla \cdot i_1 + \nabla \cdot i_2 = 0 \qquad [A\text{-}4]$$

Surface reaction rate and transfer current (neglecting the double-layer charging effects)

$$\nabla \cdot i_2 = a_i F j_{n,i} \qquad [A\text{-}5]$$

Surface reaction rate

$$j_{n,i} = k_i C^{\alpha_a} (c_{s,i}^t - c_{s,i})^{\alpha_a} c_{s,i}^{\alpha_c} \left\{ \exp\left[\frac{\alpha_a F}{RT}(\phi_1 - \phi_2 - U_i)\right] - \exp\left[-\frac{\alpha_c F}{RT}(\phi_1 - \phi_2 - U_i)\right] \right\} \qquad [A\text{-}6]$$

Solid-state diffusion equation with parabolic approximation[15,16]

$$\frac{\partial c_{s,i}^{ave}}{\partial t} = -3 a_i j_{n,i} \qquad [A\text{-}7]$$

$$c_{s,i}^{ave} - c_{s,i,Rs} = \frac{a_i j_{n,i} R_{s,i}}{5 D_{s,i}} \qquad [A\text{-}8]$$

Thermal balance[8]

$$\rho_i C_{p,i} \frac{\partial T}{\partial t} = \nabla \cdot (\lambda_i \nabla T) + q \qquad [A\text{-}9]$$

where

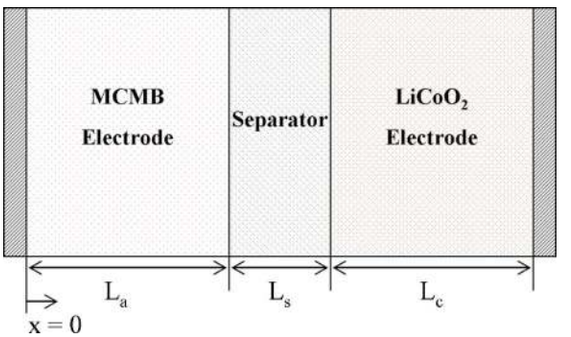

Figure A-1. (Color online) Schematic diagram of the lithium-ion cell.

$$q = F a_i j_{n,i}(\phi_1 - \phi_2 - U_i) + F a_i j_{n,i} T \frac{\partial U_i}{\partial T} + \sigma_i \nabla \phi_1 \cdot \nabla \phi_1 + \kappa_i \nabla \phi_2 \cdot \nabla \phi_2 + \frac{2\kappa_i RT}{F} V \frac{1}{C} \nabla C \cdot \nabla \phi_2 \qquad [A\text{-}10]$$

Boundary conditions.— Table A-I gives the boundary conditions required to solve the governing equations. (See Fig. A-1).

Appendix B

The temperature and concentration dependence of salt-diffusion coefficient and ionic conductivity of the bulk electrolyte reported by Valoen et al.[8] as given below are used in this paper

$$D_{e,bulk} = 1 \times 10^{-4} 10^{[-4.43 - 54/T - 0.005C - 229 - 2.2 \times 10^{-4} C]} \qquad [B\text{-}1]$$

$$\kappa_{bulk} = 1 \times 10^{-4} C[-10.5 + 0.074T - 6.96 \times 10^{-5} T^2 + 6.68 \times 10^{-4} - 1.78 \times 10^{-5} CT + 2.8 \times 10^{-5} CT^2 + 4.94 \times 10^{-7} C^2 - 8.86 \times 10^{-7} C^2 T]^2 \qquad [B\text{-}2]$$

These bulk values were corrected for the porosity and tortuosity effects for anode, separator, and cathode regions using the Bruggeman's relationships as given below

$$D_i = D_{e,bulk} \varepsilon_i^{brug_i} \qquad [B\text{-}3]$$

and

$$\kappa_i = \kappa_{bulk} \varepsilon_i^{brug_i} \qquad [B\text{-}4]$$

List of Symbols

a_i	specific surface area of porous region i, m^2/m^3
$brug_i$	Bruggeman's factor for porous region i
C	solution-phase concentration, mol/m^3
$C_{p,i}$	average specific heat conductivity of porous region i, J/kg/K
$c_{s,i}^{ave}$	solid-phase average concentration, mol/m^3
$c_{s,i,Rs}$	solid-phase surface concentration, mol/m^3
$c_{s,i}^t$	theoretical maximum concentration in solid phase, mol/m^3
$D_{e,bulk}$	salt-diffusion coefficient of bulk electrolyte, m^2/s
D_i	salt-diffusion coefficient corrected for porosity and tortuosity for region i, m^2/s
$D_{s,i}$	diffusion coefficient of Li in solid phase i, m^2/s
$f_\pm$	mean molar salt activity coefficient
F	Faraday's constant, 96487 C/equivalent
h	heat-treatment coefficient, $W/m^2/K$
i_1	solid-phase current density, A/m^2
i_2	liquid-phase current density, A/m^2

Table A-I. Boundary conditions for the lithium-ion model.

Variable	Current collector/anode ($x = 0$)	Anode/separator ($x = L_a$)	Separator/cathode ($x = L_a + L_s$)	Cathode/current collector ($x = L_a + L_s + L_c$)
C	$\nabla C = 0$	$-D_n \nabla C = -D_s \nabla C$	$-D_s \nabla C = -D_p \nabla C$	$\nabla C = 0$
ϕ_2	$i_2 = 0$	$i_2 = I_{app}$	$i_2 = I_{app}$	$i_2 = 0$
ϕ_1	$\phi_1 = 0$	$\sigma_n \nabla \phi_1 = 0$	$\sigma_p \nabla \phi_1 = 0$	$\sigma_p \nabla \phi_1 = I_{app}$
T	$-\lambda_n \nabla T = h(T - T_a)$	$-\lambda_n \nabla T = -\lambda_s \nabla T$	$-\lambda_s \nabla T = -\lambda_p \nabla T$	$-\lambda_p \nabla T = h(T - T_a)$

I_{app}	applied current density, A/m^2
$j_{n,i}$	surface reaction rate, mol/m^2/s
k_i	surface electrochemical reaction-rate constant, mol$^{-3/2}$ m$^{-1/2}$ s^{-1}
L	total thickness of the cell, m
q	rate of heat generation, W/m^3
R	ideal gas constant, 8.314 J/mol/K
$R_{s,i}$	particle radius, m
t^+	cationic transference number
T	temperature, K
t	time, s
U_i	open-circuit potential of electrode i, V vs Li/Li$^+$
V	thermodynamic factor as defined by Eq. A-2b
α_c	cathodic transfer coefficient of surface reaction
α_a	anodic transfer coefficient of surface reaction
ε_i	porosity of region i
κ_{bulk}	bulk ionic conductivity of electrolyte, S/m
κ_i	ionic conductivity corrected for porosity and tortuosity of porous region i, S/m
λ_i	average thermal conductivity of porous region i, W/m/K
ρ_i	average density of porous region i, kg/m^3
σ_i	electronic conductivity of solid phase i, S/m
ϕ_1	solid-phase potential, V
ϕ_2	liquid-phase potential, V

Subscripts

1	solid phase of the porous region
2	liquid phase of the porous region
bulk	bulk electrolyte
e	electrolyte phase
i	anode, separator, or cathode region

Superscripts

ave	average over the solid electrode particle
t	total theoretical electrode capacity

References

1. M. Doyle, J. Newman, A. S. Gozdz, C. N. Schmutz, and J. M. Tarascon, *J. Electrochem. Soc.*, **143**, 1890 (1996).
2. P. Arora, M. Doyle, A. S. Gozdz, R. E. White, and J. Newman, *J. Power Sources*, **88**, 219 (2000).
3. M. Doyle and Y. Fuentes, *J. Electrochem. Soc.*, **150**, A706 (2003).
4. V. Srinivasan and J. Newman, *J. Electrochem. Soc.*, **151**, A1517 (2004).
5. J. Christensen, V. Srinivasan, and J. Newman, *J. Electrochem. Soc.*, **153**, A560 (2006).
6. G. Botte, B. A. Johnson, and R. E. White, *J. Electrochem. Soc.*, **146**, 914 (1999).
7. V. Srinivasan and C. Y. Wang, *J. Electrochem. Soc.*, **150**, A98 (2003).
8. L. O. Valoen and J. N. Reimers, *J. Electrochem. Soc.*, **152**, A882 (2005).
9. M. Doyle, T. F. Fuller, and J. Newman, *J. Electrochem. Soc.*, **140**, 1526 (1993).
10. W. B. Gu and C. Y. Wang, *J. Electrochem. Soc.*, **147**, 2910 (2000).
11. K. E. Thomas and J. Newman, *J. Power Sources*, **119–121**, 844 (2003).
12. Y. Reynier, R. Yazami, and B. Fultz, *J. Power Sources*, **119–121**, 850 (2003).
13. K. Kumaresan, Q. Guo, P. Ramadass, and R. E. White, *J. Power Sources*, **158**, 679 (2006).
14. T. F. Fuller, M. Doyle, and J. Newman, *J. Electrochem. Soc.*, **141**, 1 (1994).
15. C. Y. Wang, W. B. Gu, and B. Y. Liaw, *J. Electrochem. Soc.*, **145**, 3407 (1998).
16. V. R. Subramanian, J. A. Ritter, and R. E. White, *J. Electrochem. Soc.*, **148**, E444 (2001).